Lawrence Berkeley National Laboratory
Lawrence Berkeley National Laboratory

Title
Structural Properties of Ge Nanocrystals Embedded in Sapphire

Permalink
https://escholarship.org/uc/item/82r728n5

Authors
Sharp, I.D.
Xu, Q.
Yi, D.O.
et al.

Publication Date
2008-06-20

Peer reviewed

eScholarship.org Powered by the California Digital Library
University of California

Structural Properties of Ge Nanocrystals Embedded in Sapphire

I.D. Sharp and Q. Xu

Materials Sciences Division, Lawrence Berkeley National Laboratory, Berkeley, CA 94720 and Department of Materials Science and Engineering, University of California, Berkeley, CA 94720

D.O. Yi

Lawrence Livermore National Laboratory, Livermore, CA 94550

C.W. Yuan

Materials Sciences Division, Lawrence Berkeley National Laboratory, Berkeley, CA 94720 and Department of Materials Science and Engineering, University of California, Berkeley, CA 94720

J.W. Beeman, K.M. Yu, and J.W. Ager III

Materials Sciences Division, Lawrence Berkeley National Laboratory, Berkeley, CA 94720

D.C. Chrzan and E.E. Haller

Materials Sciences Division, Lawrence Berkeley National Laboratory, Berkeley, CA 94720 and Department of Materials Science and Engineering, University of California, Berkeley, CA 94720

ABSTRACT

Isotopically pure ^{74}Ge nanocrystals were formed in a sapphire matrix by the ion beam synthesis method. In contrast to those embedded in amorphous silica, sapphire-embedded nanocrystals are clearly faceted and are preferentially oriented with respect to the crystalline matrix. *In situ* transmission electron microscopy of heated samples reveals that the nanocrystals melt at 955 °C ± 15 °C, very near to the bulk Ge melting point. Raman spectra indicate that the sapphire-embedded Ge nanocrystals are under compressive stress in the range of 3 - 4 GPa. The

magnitude of the stress is consistent with that expected for hydrostatic pressure arising from solidification. Stress relaxation was not observed for sapphire-embedded Ge nanocrystals; this is attributed to the slow self-diffusion rate of the alumina matrix atoms at temperatures below the nanocrystal melting point.

PACS numbers: 81.07.-b, 61.46.Hk, 78.30.-j, 62.25.+g,

I. INTRODUCTION

Ge nanocrystals have been studied extensively in recent years and have been suggested for use in nonvolatile memory and integrated optoelectronic devices. The majority of this work has focused on nanocrystals embedded in silica matrices because of the technological importance and wide availability of this material. However, a few studies have reported on Ge nanocrystals embedded in other matrix materials such as Al_2O_3,[1] SiC,[2] AlN,[3] and HfAlO.[4] Because the surfaces and interfaces of nanoscale materials can play a dominant role in determining their properties, it is interesting to compare the properties of nanocrystals embedded in different matrices. For example, though quantum mechanical models predict efficient size-dependent photoluminescence from group IV semiconductor nanocrystals, the reported luminescence from silica-embedded Ge nanocrystals has mostly been attributed to defects within the oxide or at the oxide/nanocrystal interface.[5] Replacement of the matrix with a different material changes the nature of the defects at the nanocrystal/matrix interface and should provide information on the recombination mechanism. In this report, we examine the structural properties of Ge nanocrystals embedded in sapphire and, when appropriate, compare their properties to those in the well-studied system of silica-embedded Ge nanocrystals.

The optical properties of Ge nanoclusters embedded in sapphire have been studied both theoretically[6] and experimentally.[7-9] However, fewer reports on the structural properties of this materials system are available. Budai and co-workers formed Ge nanoparticles in sapphire matrices and examined the influence of substrate temperature, dose, and annealing conditions on the resulting nanocrystals.[1] They found that amorphization of the substrate followed by recrystallization of γ-Al_2O_3 from the original α-Al_2O_3 could be utilized to alter orientation relationships between nanocrystals and matrix as well as the particle size distribution. In the

present case, the implantation temperature is high enough and the dose is low enough that nanocrystals nucleate and grow within α-Al_2O_3. Here, we further study the structural properties of this materials system to determine orientation relationships between the matrix and nanocrystals, the melting point of embedded nanocrystals, faceting, and stress generation mechanisms. Our findings suggest that nanocrystals grow in the liquid phase and that significant stresses accumulate within the nanocrystals due to the solid-liquid phase transformation during cooling.

II. EXPERIMENTAL DETAILS

Isotopically pure ^{74}Ge nanocrystals were formed by multi-energy ion implantation at 150 keV to 8×10^{15} cm^{-2}, 120 keV to 6×10^{15} cm^{-2}, 80 keV to 5×10^{15} cm^{-2}, and 50 keV to 3×10^{15} cm^{-2} followed by thermal annealing in sealed ampoules at 1200 °C for 1h under Ar. Annealing was terminated by rapid quenching of the sealed ampoules under running cold water. Post growth thermal annealing was also performed under Ar at temperatures below 1200 °C.

Ge concentration profiles were obtained using Rutherford backscattering spectrometry (RBS) with a 1.92 MeV He^+ beam and a sample tilt of 50° to improve depth resolution. Backscattered ions were collected at an angle of 165° with a Si surface barrier detector. Raman spectroscopy was performed using the 488 nm line from an Ar^+ laser in a macroscopic optical setup with ~5 cm^{-1} resolution. Transmission electron microscopy (TEM) was performed on as-grown samples to determine the structures of nanocrystals and their size distributions. Both cross-sectional and plan view samples were prepared in the standard fashion and micrographs were obtained using Philips CM200 & CM300 microscopes as well as a JEOL 3010. *In situ* TEM studies of the melting point of sapphire-embedded Ge nanocrystals were performed between room temperature and 1000 °C ± 15 °C using a Gatan 628Ta single-tilt heating stage in

a JEOL 3010 electron microscope operating at 300 keV. Direct *in situ* measurement of the diffraction patterns from Ge nanocrystals was not feasible due to the comparatively high intensity diffraction of the sapphire substrate. Therefore, bright field and dark field micrographs were recorded *in situ* at 15 °C steps every 5 min with beam currents of no more than 8 μA to minimize sample heating. Melting was defined by the disappearance of contrast in dark field images which indicates the loss of crystallinity of nanoparticles.

III. RESULTS AND DISCUSSION

A. Rutherford Backscattering Spectrometry

Figure 1 shows Ge concentration profiles obtained by RBS after implantation both before and after thermal annealing. Prior to annealing, the Ge peak concentration is ~3 at. % located approximately 40 nm below the surface of the sample. Subsequent to annealing at 1200 °C for 1 h, the total Ge content is reduced from 1.95×10^{16} cm^{-2} to 1.6×10^{16} cm^{-2} and the peak shifts deeper into the sample due to out-diffusion of Ge from the surface during annealing. The asymmetric evolution of the Ge concentration profile suggests that implantation damage may lead to a depth-dependent diffusion coefficient. Additional growth attempts at higher temperatures (up to 1600 °C in a high temperature vacuum furnace) resulted in nearly complete out-diffusion of Ge from the sapphire substrate that suppressed nanocrystal formation. These results demonstrate that successful nanocrystal synthesis in sapphire relies on a balance between the implant and annealing conditions. In particular, low energy implantation or very high temperature annealing may lead to significant diffusional losses of Ge that prohibit nanocrystal formation near the surface. However, under the present conditions, nanocrystal formation is observed.

B. Transmission Electron Microscopy

Figure 2(a) shows a cross-sectional TEM image of the near surface region of an implanted and annealed sample. Significant strain fields in the implanted zone remain after annealing, as evidenced by the dark contrast in the 60 nm closest to the surface. Further below the surface, end-of-range damage from Ge implantation is also observed. These high contrast stress fields obscure the low magnification electron micrographs of Ge nanocrystals. However, under higher magnification, moiré fringes arising from the overlap of sapphire and Ge crystal planes are observed, as shown in Fig. 2(b). The existence of the moiré fringes indicates that not only are the Ge nanoparticles crystalline, but that the matrix also remains crystalline and recovers much of the implantation damage after thermal annealing.

Because the stress fields prevent low magnification electron microscopy and simultaneous imaging of large nanocrystal ensembles, the size distribution was obtained by measurements of nanocrystals at a relatively high magnification. Figure 3 shows the size distribution obtained in this manner. Unlike the near-Gaussian distribution typical of ion beam synthesized nanocrystals in silica, the distribution of those embedded in sapphire is nearly log-normal. The unusual distribution shape is a consequence of the depth dependence on nanocrystal sizes. The larger nanocrystals lie predominantly near the position of the maximum Ge concentration, whereas the smaller crystals are located primarily in the depth range between the surface and the large clusters. Although further work is required to precisely determine the mechanism of formation of these spatially size segregated nanocrystals, it may be that out-diffusion of Ge from the surface reduces crystal sizes in regions near the surface. Additionally, implantation damage could lead to depth dependent diffusivities that spatially influence the nucleation and growth rates.

The structure of sapphire-embedded Ge nanocrystals was revealed through HR-TEM. Ge nanocrystals embedded in amorphous silica are characterized by spherical shapes with no clear faceting. However, those embedded in sapphire exhibit clearly defined facets, as shown in Fig. 4. Nanocrystal synthesis is performed at 1200 °C, well above the bulk Ge melting point of 936 °C, and *in situ* heating measurements (described below) indicate that Ge nanoparticles are liquid at the growth temperature. Therefore, the facets of the nanocrystals are determined at the growth temperature by the interface energies between liquid Ge and the individual sapphire crystal planes.

The nanocrystal in Fig. 4 is partially exposed as a result of thinning during TEM sample preparation. The crystal structure of the sapphire substrate is clearly visible, along with that of the Ge nanocrystal (upper left region of the nanocrystal). Moiré fringes are also visible in the lower right region of the nanocrystal. Fast Fourier transformation (FFT) in the sapphire substrate region, the Ge nanocrystal region (Ge crystal planes only), and the moiré fringe (overlapping nanocrystal and substrate) region reveals an invariant orientation relationship between Ge nanocrystals and the sapphire matrix with $(111)_{Ge} \parallel (\bar{1}104)_{sapphire}$. From this analysis, it is not yet possible to determine the interface normal vector.

In situ heating and cooling experiments were performed to determine the melting points of sapphire-embedded Ge nanocrystals. It is well known that nanocrystals exhibit size-dependent melting points as a consequence of the increasing contribution of the surface/interfacial free energy to the total energy of nanoparticles with decreasing crystal size.[10,11] For the case of free standing nanocrystals, a melting point depression occurs that varies inversely with the particle radius. However, for the case of embedded nanocrystals, melting point depression, enhancement, and even hysteresis are possible.[12] In the present study, the

melting point determination is made based on the disappearance of individual nanocrystals in the dark field (DF) view. Using this technique, we find that the sapphire-embedded nanocrystals melt at 955 °C ± 15 °C, which is close to the bulk melting point of 936 °C. Upon cooling from the molten state, resolidification is also observed at 955 °C ± 15 °C . Considering the experimental temperature measurement limitations, the melting point of nanocrystals is indiscernible from that of bulk Ge. The observation that melting and solidification occur very close to the bulk melting point suggests that the solid Ge/sapphire and liquid Ge/sapphire interface energies are similar in magnitude and that neither melting nor solidification are kinetically hindered.[12]

C. Raman Spectroscopy

Additional quantitative structural analysis was achieved by Raman spectroscopy. Raman spectra of nanocrystals are characterized by size dependent phonon confinement effects which, for the case of Si and Ge, are manifested by asymmetric line broadening and red shifting due to breakdown of the $\vec{k} = 0$ selection rule for Stokes scattering.[13,14] Figure 5 shows the Raman spectrum of an isotopically enriched ^{74}Ge bulk crystal along with the spectrum from isotopically pure ^{74}Ge nanocrystals embedded in sapphire. The nanocrystal spectrum exhibits the expected asymmetric broadening due to phonon confinement. However, the spectrum is considerably blue shifted with respect to that of the bulk reference spectrum, in disagreement with the predictions of phonon confinement theory. A similar, though smaller, blue shift of Raman spectra of silica-embedded Ge nanocrystals is frequently observed and is attributed to matrix-induced compressive stress on embedded nanocrystals.[15-20]

i. Quantitative Stress Analysis

It has been suggested that stresses on silica-embedded Ge nanocrystals arise from solidification expansion upon cooling from the growth temperature.[21,22] Here, growth is performed well above the melting point of the Ge nanocrystals so that Ge clusters grow as molten nanodroplets that solidify in sapphire upon rapid cooling. Because solid Ge has a lower density than liquid Ge, the resulting solid nanoparticles are larger than the sapphire matrix cavities and they are under compressive stress. Additionally, the difference in thermal expansion coefficients results in a different extent of contraction for sapphire and Ge that contributes to the stress in the nanocrystal at room temperature.

A variety of methods exist for determining the stress state of a material. In particular, x-ray and electron diffraction provide direct measurements of the lattice parameter, thereby giving the most fundamental measures of stress. In the present case, however, the small sizes of the nanocrystals, their broad size distribution, and the diminutive total volume of nanocrystalline material limit the diffraction resolution required to discern small changes of the lattice parameter with compression. Although it is a less direct measure of stress, Raman spectroscopy provides both the sensitivity and resolution required to determine stresses on nanocrystals.

Cerdeira *et al*. derived an expression to relate the hydrostatic pressure, P, on a material to the change of the Raman shift.[23] Here, we use a slightly modified form of this equation that is applicable for nanocrystals under compressive stress:[15]

$$P = \frac{\omega_{stressed} - \omega_{relaxed}}{3\gamma\omega_0\left(S_{11} + 2S_{12}\right)} \qquad [1]$$

where $\omega_{stressed}$, $\omega_{relaxed}$, and ω_0 are the Raman shifts of stressed nanocrystals embedded in sapphire, relaxed nanocrystals calculated according to phonon confinement theory, and the

isotopically enriched bulk ^{74}Ge reference sample, respectively. S_{ij} is the *ij*th element of the elastic compliance tensor and γ is the mode-Grüneisen parameter.

For the case of Ge nanocrystals embedded in silica, the relaxed Raman line position, $\omega_{relaxed}$, was previously determined by measurement of exposed nanocrystals after selective etching of the matrix.[15,24] However, in the present case, no suitable selective etchant is available so it is not possible to directly measure the relaxed state as a reference. Therefore, the relaxed line position is calculated using the commonly utilized phonon confinement model developed by Richter *et al*.[25] The functional form for the Raman intensity, *I*, as a function of frequency, ω, for a system exhibiting phonon confinement is:

$$I(\omega) = \int \frac{|C(0,k)|^2}{(\omega - \overline{\omega}(k)) + \left(\frac{\Gamma_0}{2}\right)^2} d^3k \qquad [2]$$

where $\overline{\omega}(k)$ is the average optical phonon dispersion relation over the Brillouin zone, Γ_0 is the bulk natural line width, and $C(0,k)$ are the Fourier coefficients associated with the phonon weighting function. We note that the calculated Raman line shape is extremely sensitive to the precise choice of the phonon weighting function, $W(r,L)$. However, the Gaussian weighting function proposed by Campbell and Fauchet[26] describes the Raman spectra of Ge nanocrystals embedded in silica well. Therefore, we choose the phonon weighting function of the form:

$$W(r,L) = \exp\left(-8\pi^2 r^2 / L^2\right) \qquad [3]$$

with the associated Fourier coefficients:

$$|C(0,k)|^2 \cong \exp\left(-k^2 L^2 / 16\pi^2\right) \qquad [4]$$

where *L* is the nanocrystal diameter. This choice of the phonon weighting function drives the surface vibrational amplitude close to zero due to the matrix-induced fixed boundary condition

and is consistent with recent dynamical matrix calculations for Ge nanocrystals.[14] An expression for the average phonon dispersion of Ge within the Brillouin zone, $\overline{\omega}(k)$, was calculated by Wellner and co-workers using the Brout sum method and neutron scattering data of Nilsson and Nelin to be:[21]

$$\overline{\omega}(k) = \left(\omega_0^2 - \frac{43565 k_r^2}{|k_r| + 0.5766} \right)^{1/2} \qquad [5]$$

where $k_r = (a/2\pi)k$ is the reduced wavevector, a = 0.566 nm is the lattice parameter of bulk Ge, and ω_0 is the bulk zone center optical phonon frequency for isotopically enriched bulk ^{74}Ge.

Figure 5(b) shows the experimental Raman spectrum along with a simulated spectrum (dashed line) calculated according to Eq. 2 with Fourier coefficients and phonon dispersion curve given by Eqs. 4 & 5, respectively. The finite particle size distribution is accounted for by direct summation of normalized simulated spectra of different sizes weighted by the measured size distribution. This simulated spectrum shows the expectation for fully relaxed nanocrystals and gives a line position red shifted in relation to the bulk reference spectrum, in accordance with the expectations of the phonon confinement model.

We can estimate the contribution to the total compressive stress on nanocrystals from solidification and differential thermal expansion by using continuum elasticity theory and an assumed, simplified geometry. An individual nanocrystal is modeled as an elastically isotropic spherical precipitate of radius R_{Ge} confined within a spherical matrix cavity of radius $R_{Al_2O_3}$ in sapphire. We also assume that the sapphire matrix is elastically isotropic. The nanocrystal surface is assumed to be in direct contact with the sapphire at all times, and the nanocrystal mass is held constant. Given these assumptions, the pressure in the nanocrystal at the annealing

temperature can be calculated in terms of the elastic properties of the Ge and sapphire, and Ge/sapphire surface tension:

$$P_{Ge} = \frac{12 B_{Ge} \mu_{Al_2O_3} [R_{Ge} - R_{Al_2O_3}] + 3 B_{Ge} 2 \gamma_{Ge-Al_2O_3} R_{Al_2O_3} / R_{Ge}}{4 \mu_{Al_2O_3} R_{Ge} + 3 B_{Ge} R_{Al_2O_3}} \quad [6]$$

where $\mu_{Al_2O_3}$ and B_{Ge} are the shear modulus of sapphire and the bulk modulus of Ge, respectively, and $\gamma_{Ge-Al_2O_3}$ is the Ge/sapphire interface energy. To our knowledge, the solid Ge-sapphire interface energy is not known. We use a value of 1.3 J/m^2 for $\gamma_{Ge-Al_2O_3}$, which is the liquid Ge-sapphire interface energy calculated from the wetting angle measurements of Kaiser and co-workers.[27] Significant differences between the liquid Ge-sapphire interface energy and the solid Ge-sapphire interface energy would result in large deviations of the melting point of nanocrystals from the bulk melting point which are not observed during *in situ* TEM heating measurements.

The pressure in the nanocrystal is measured via Raman spectroscopy at room temperature, so one must take into account the coefficient of thermal expansion for Ge and sapphire and the volumetric change of Ge due to solidification by replacing the radii in Eq. 6 by:

$$\begin{aligned} R_{Al_2O_3} &= R^0_{Al_2O_3} \left(1 + (T_{meas} - T_a) \alpha_{Al_2O_3}\right) \\ R_{Ge} &= R^0_{Ge} \left(1 + (T_m - T_a) \alpha_{Ge(L)} + (T_{meas} - T_m) \alpha_{Ge(S)}\right) \left(V_s / V_L\right)^{1/3} \end{aligned} \quad [7]$$

where the superscript of 0 indicates the radii are taken at the annealing temperature, T_a. T_m is the measured melting point of the nanocrystals (955 °C), and measurement is performed at room temperature, T_{meas}. Bulk values for the thermal expansion coefficient of solid Ge ($\alpha_{Ge(s)}$), molten Ge ($\alpha_{Ge(L)}$), and sapphire ($\alpha_{Al_2O_3}$) are assumed. The volumetric expansion of Ge liquid to solid is 6%.[21,28]

The solid curve in Fig. 5(b) shows the simulated spectrum calculated using the phonon confinement model after accounting for stress originating from the interface energy, solidification expansion, and differential thermal expansion. The spectrum is calculated in the same manner as that given by the dashed line, but the spectral contributions from each nanocrystal size are shifted according to Eq. 1 using the compressive stresses calculated by Eq. 6. Together, solidification and differential thermal expansion lead to 2.5 GPa of compressive stress, independent of particle size, that results in a 8.8 cm^{-1} blue shift of the Raman spectrum. We note that the contribution from differential thermal expansion leads to a reduction of the total stress. The interface energy contributes a size dependent compressive stress equivalent to $2\gamma_{Ge/Al_2O_3}/r$ which leads to an additional blue shift and some sharpening of the spectrum.

Although the stress calculations presented above rely on the approximation of a spherical particle in an elastically isotropic matrix, the agreement between theory and experiment is quite good. Therefore, we conclude that the observed blue shift of the Raman spectrum is primarily a consequence of the volumetric expansion of Ge during solidification upon cooling from the growth temperature, differential thermal expansion, and the Gibbs-Thomson effect. Although, non-hydrostatic stress components may be present due to interface registry between Ge nanocrystals and the sapphire matrix, these contributions to the total stress are found to be negligible.

ii. Stress Relaxation

We recently demonstrated that Ge nanocrystals embedded in silica are under compressive stress and that this stress can be controllably relaxed via post growth thermal annealing.[15] Stress relaxation occurs by the thermally activated diffusive flux of matrix atoms away from local regions of nanocrystal growth. In the present study, we attempted to relax the observed

compressive stress by post-growth thermal annealing at temperatures both above and below the nanocrystal melting point (955 °C). Figure 6(a) shows Raman spectra of sapphire embedded Ge nanocrystals in the as-grown state and after post-growth thermal annealing at 800 °C for 72 h and 1100 °C for 24 h. No stress relaxation is observed after either post annealing treatment. Indeed, compressive stress increases after annealing at 1100 °C. These observations are consistent with the diffusive stress relaxation mechanism observed for silica-embedded Ge nanocrystals and with the stress origin described in the previous section. We further note that the surface phonon boundary condition does not change during post-growth thermal annealing.[14]

During annealing at 800 °C the Ge nanoparticles remain crystalline and are compressively strained such that a driving force exists for stress relaxation. However, at this temperature self-diffusion within sapphire is exceptionally slow ($D_O \sim 10^{-28}$ cm^2 s^{-1}).[29] Therefore, even after a heating period of 72 h, no observable stress relaxation has occurred. At 1100 °C oxygen self-diffusion ($D_O \sim 10^{-22}$ cm^2 s^{-1})[29] should be rapid enough to permit observable stress-relaxation after 24 h. However, at this temperature Ge nanoparticles are molten and contraction of Ge upon melting removes the compressive strain, and thus driving force for relaxation, at the annealing temperature. The increase of stress after annealing at 1100 °C is a consequence of the differential thermal expansion between liquid Ge and sapphire. During annealing, diffusion is sufficient for the molten nanodroplets and the sapphire cavity to reach the equilibrium radius. Upon cooling, stresses again accumulate due to solidification and differential thermal expansion. Figure 6(b) shows the simulated Raman spectrum which accounts for compressive stress after annealing with T_a = 1100 °C. Once again, experiment and theory agree well and the stress generation model is sufficient to describe the observed stress. We therefore

conclude that the stress enhancement after 1100 °C post-growth thermal annealing is a consequence of differential thermal expansion.

IV. CONCLUSION

In conclusion, we synthesized ^{74}Ge nanocrystals in sapphire by ion implantation followed by thermal annealing at 1200 °C. The structural properties of these nanocrystals possess both differences and similarities compared to those embedded in amorphous silica. Sapphire embedded nanocrystals are highly faceted and have an invariant orientation relationship to the sapphire matrix with $(111)_{Ge} \parallel (\bar{1}104)_{sapphire}$. *In situ* heating in a TEM reveals that the nanocrystals melt and re-solidify near the bulk melting point. Raman spectra are well described by a phonon confinement model, but the line positions are blue shifted with respect to bulk as a consequence of significant compressive stresses. Calculations utilizing continuum elasticity theory reveal that the compressive stress can be fully accounted for by solidification expansion upon cooling of molten nanodroplets from the growth temperature, differential thermal expansion, and the Gibbs-Thomson effect. Stress relaxation, which should occur via diffusion of matrix atoms, does not occur over reasonable time scales because of the exceptionally slow motion of self-atoms at temperatures below the melting point of nanocrystals. Above the melting point, the driving force for relaxation disappears as a consequence of contraction of Ge upon melting. Because nanocrystals have significant potential for use in memory devices, and would therefore be embedded in very thin dielectric films, it is of great importance to understand stresses that may accumulate during growth. Here, we have shown how such stresses may accumulate as a consequence of a phase change between the growth temperature and room temperature. Optical measurements of sapphire-embedded Ge nanocrystals, which are beyond

the scope of the present work, are underway and initial results indicate that defect levels are responsible for broad, visible luminescence.

ACKNOWLEDGEMENTS

I.D.S. acknowledges support from the Intel Robert N. Noyce fellowship. Q.X. acknowledges support through a U.C. Berkeley Fellowship. D.C.C. and E.E.H. acknowledge support from the Miller Institute for Basic Research in Science. This work is supported in part by the Director, Office of Science, Office of Basic Energy Sciences, Division of Materials Science and Engineering, of the U.S. Department of Energy under contract No. DE-AC02-05CH11231 and in part by U.S. NSF Grant No. DMR-0405472. Electron microscopy was performed at the National Center for Electron Microscopy, LBNL.

REFERENCES

[1] J. D. Budai, C. W. White, S. P. Withrow, M. F. Chisholm, J. Zhu, and R. A. Zuhr, Nature **390,** 384 (1997).

[2] A. Hedler, S. Urban, T. Kups, U. Kaiser, and W. Wesch, Nucl. Instrum. Methods B **248,** 337 (2004).

[3] K. M. Hassan, A. K. Sharma, J. Narayan, J. F. Muth, C. W. Teng, and R. M. Kolbas, Appl. Phys. Lett. **75,** 1222 (1999).

[4] Y. Q. Wang, J. H. Chen, W. J. Yoo, S. J. Kim, R. Gupta, Z. Y. L. Tan, D.-L. Kwong, A. Y. Du, and N. Balasubramanian, Appl. Phys. Lett. **84,** 5407 (2004).

[5] L. Rebohle, J. v. Borany, H. Fröb, and W. Skorupa, Appl. Phys. B **71,** 131 (2000).

[6] H.-C. Weissker, J. Furthmueller, and F. Bechstedt, Phys. Rev. B **65,** 155328 (2002).

[7] P. Tognini, A. Stella, S. D. Silvestri, M. Nisoli, S. Stagira, P. Cheyssac, and R. Kofman, Appl. Phys. Letters **75,** 208 (1999).

[8] P. Tognini, L. C. Andreani, M. Geddo, A. Stella, P. Cheyssac, R. Koffman, and A. Migliori, Phys. Rev. B **53,** 6992 (1996).

[9] Q. Wan, C. L. Lin, N. L. Zhang, W. L. Liu, G. Yang, and T. H. Wang, Appl. Phys. Lett. **82,** 3162 (2003).

[10] P. Buffat and J.-P. Borel, Phys. Rev. A **13,** 2287 (1976).

[11] A. N. Goldstein, C. M. Echer, and A. P. Alivisatos, Science **256,** 1425 (1992).

[12] Q. Xu, I. D. Sharp, C. W. Yuan, D. O. Yi, C. Y. Liao, A. M. Glaeser, A. M. Minor, J. W. Beeman, M. C. Ridgway, P. Kluth, J. W. A. III, D. C. Chrzan, and E. E. Haller, submitted (2006).

[13] W. Cheng and S.-F. Ren, Phys. Rev. B **65,** 205305 (2002).

[14] S.-F. Ren and W. Cheng, Phys. Rev. B **66,** 205328 (2002).

[15] I. D. Sharp, D. O. Yi, Q. Xu, C. Y. Liao, J. W. A. III, J. W. Beeman, Z. Liliental-Weber, K. M. Yu, D. Zakharov, D. C. Chrzan, and E. E. Haller, Appl. Phys. Lett. **86,** 063107 (2005).

[16] A. Cheung, G. d. M. Azevedo, C. J. Glover, D. J. Llewellyn, R. G. Elliman, G. J. Foran, and M. C. Ridgeway, Appl. Phys. Lett. **84,** 278 (2004).

[17] X. L. Wu, T. Gao, X. M. Bao, F. Yan, S. S. Jiang, and D. Feng, J. Appl. Phys. **82,** 2704 (1997).

[18] W. K. Choi, V. Ng, S. P. Ng, H. H. Thio, Z. X. Shen, and W. S. Li, J. Appl. Phys. **86,** 1398 (1999).

[19] U. Serincan, G. Kartopu, A. Guennes, T. G. Finstad, R. Turan, Y. Ekinci, and S. C. Bayliss, Semicond. Sci. Technol. **19,** 247 (2004).

[20] M. Fujii, S. Hayashi, and K. Yamamoto, Jpn. J. Appl. Phys. **30,** 687 (1991).

[21] A. Wellner, V. Paillard, C. Bonafos, H. Coffin, and A. Claverie, J. Appl. Phys. **94,** 5639 (2003).

[22] J. v. Borany, R. Groetzschel, K. H. Heinig, A. Markwitz, W. Matz, B. Schmidt, and W. Skorupa, Appl. Phys. Lett. **71,** 3215 (1997).

[23] F. Cerdeira, C. J. Buchenauer, F. H. Pollak, and M. Cardona, Phys. Rev. B **5,** 580 (1972).

[24] I. D. Sharp, Q. Xu, C. Y. Liao, D. O. Yi, J. W. Beeman, Z. Liliental-Weber, K. M. Yu, D. N. Zakharov, J. W. A. III, D. C. Chrzan, and E. E. Haller, J. Appl. Phys. **97,** 124316 (2005).

[25] H. Richter, Z. P. Wang, and B. Ley, Solid State Commun. **39,** 625 (1981).

[26] I. H. Campbell and P. M. Fauchet, Solid State Commun. **58,** 739 (1986).

[27] N. Kaiser, A. Croell, F. R. Szofran, S. D. Cobb, and K. W. Benz, J. Crystal Growth **231,** 448 (2001).

[28] D. C. Emmony, N. J. Phillips, J. H. Toyer, and L. J. Willis, J. Phys. D: Appl. Phys. **8,** 1472 (1975).

[29] A. H. Heuer and K. P. D. Lagerloef, Philos. Mag. Lett. **79,** 619 (1999).

FIGURE CAPTIONS

Fig. 1: Concentration profiles of Ge in sapphire before and after nanocrystal growth at 1200 °C for 1h obtained by Rutherford backscattering spectrometry. After annealing, the total Ge content is reduced due to out-diffusion of Ge from the surface.

Fig. 2: Cross sectional TEM micrographs of an implanted and annealed sapphire sample containing Ge nanocrystals. The lower magnification micrograph (a) shows contrast arising from stress fields and end of range implantation damage. At higher magnification (b) moiré fringes become visible from the overlap of the crystal planes of Ge nanocrystals and the sapphire matrix.

Fig. 3: Size distribution of Ge nanocrystals embedded in sapphire after 1200 °C annealing for 1 h obtained by analysis of HR-TEM images.

Fig. 4: HR-TEM image of an individual partially exposed Ge nanocrystal embedded in sapphire. The upper left region of the nanocrystals shows the Ge lattice and the bottom right portion of the nanocrystal exhibits moiré fringes from the overlap of the crystal planes of the Ge nanocrystal and the crystalline sapphire substrate. FFT of the image in different regions reveals a $(111)_{Ge} \parallel (\bar{1}104)_{sapphire}$ orientation relationship between nanocrystals and the matrix.

Fig. 5: (a) Raman spectra of isotopically enriched bulk ^{74}Ge (○) and isotopically pure ^{74}Ge nanocrystals embedded in sapphire (□). The nanocrystal spectrum is blue shifted relative to the bulk reference due to compressive stress. Lines between data points are given for clarity. (b)

Raman spectrum of ^{74}Ge nanocrystals embedded in sapphire (■) compared to simulated spectra. The dashed curve is the phonon confinement simulation for the case of fully relaxed nanocrystals and the solid curve is the simulation accounting for compressive stress on nanocrystals arising from solidification expansion, the Gibbs-Thomson effect, and differential thermal expansion.

Fig. 6: (a) Raman spectra of ^{74}Ge nanocrystals: as-grown (■), after post-growth thermal annealing at 800 °C for 72 h (○), and after post-growth thermal annealing at 1100 °C for 24 h (Δ). The vertical dashed line gives the Raman line position of the bulk ^{74}Ge reference sample. Lines between data points are given for clarity. (b) Raman spectrum of ^{74}Ge nanocrystals embedded in sapphire after post-growth thermal annealing at 1100 °C for 24 h (▲). The solid curve is the phonon confinement simulation, including the shift due to stress, for growth at 1100 °C.

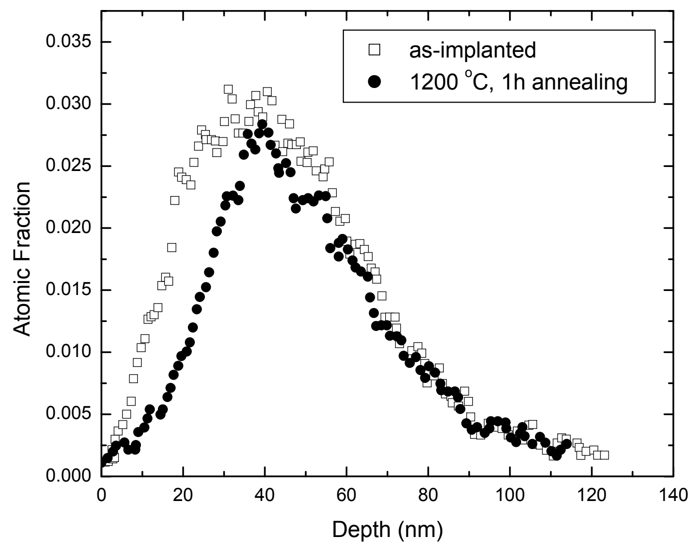

Figure 1

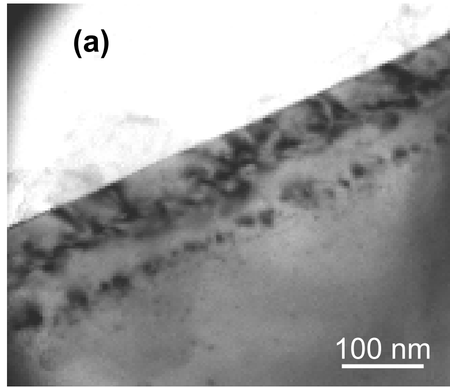

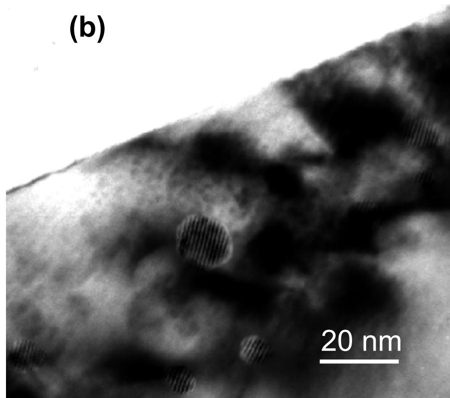

Figure 2

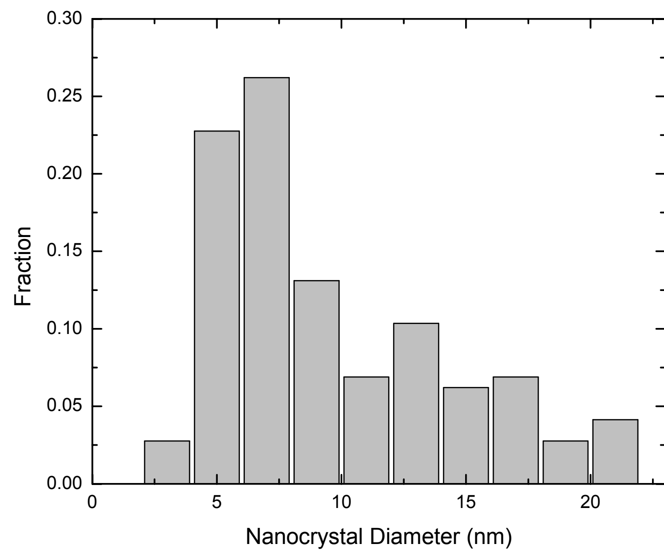

Figure 3

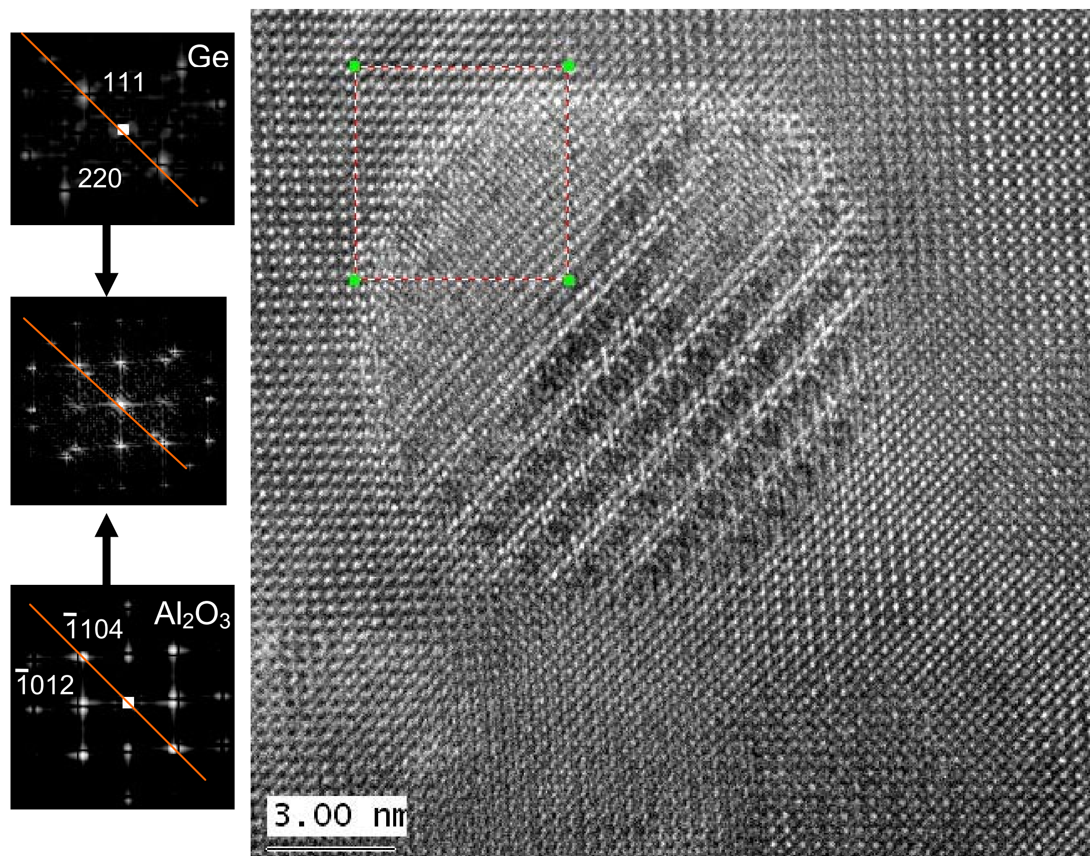

Figure 4

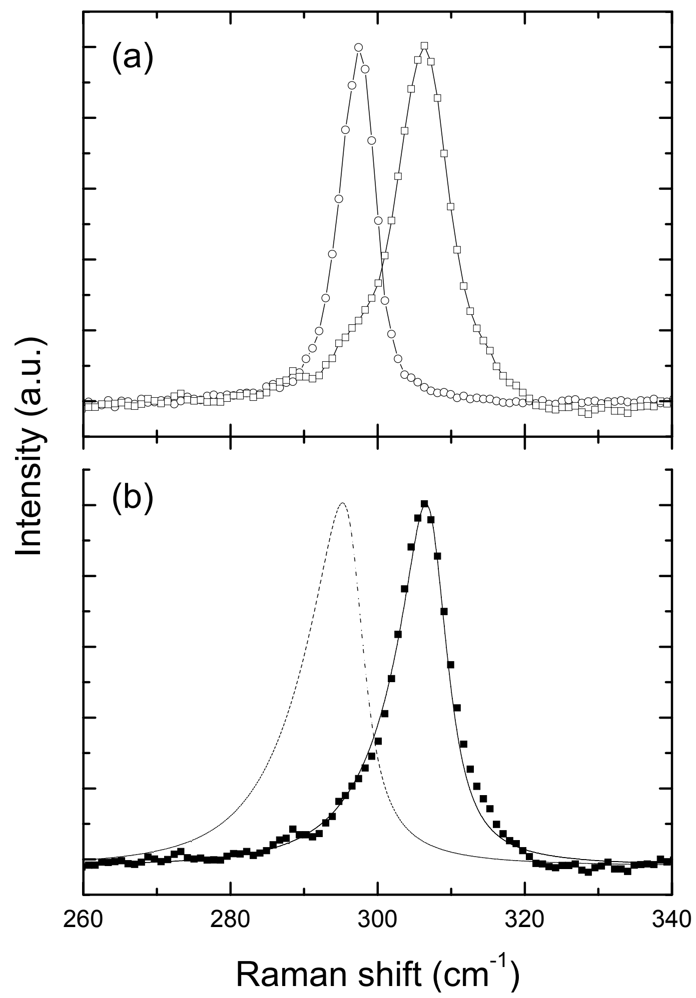

Figure 5

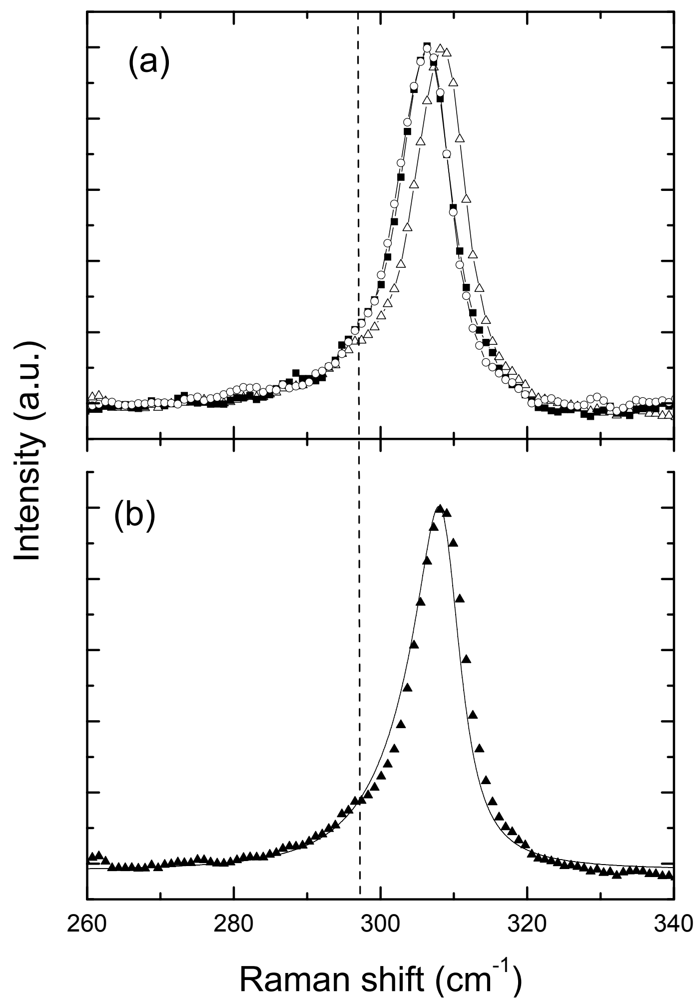

Figure 6